This is a preprint of the following article, which is available at: http://mdolab.engin.umich.edu
R. Fakhimi and M. Shahabsafa and W. Lei and S. He and J. R. R. A. Martins and L. Zuluaga and T. Terlaky. Discrete Multi-Scenario Truss Sizing Optimization: Model Analysis and Computational Methodology Experiments. *Engineering Optimization*.
The original article may differ from this preprint and is available at:
https://doi.org/10.1007/s11081-021-09672-6.

Discrete Multi-Load Truss Sizing Optimization: Model Analysis and Computational Experiments

Ramin Fakhimi, Mohammad Shahabsafa, Weiming Lei, Tamás Terlaky, and Luis F. Zuluaga
Lehigh University, Department of Industrial and Systems Engineering, Harold S. Mohler Laboratory, 200 West Packer Avenue, Bethlehem, PA 18015-1582

Sicheng He and Joaquim R. R. A. Martins
University of Michigan, Department of Aerospace Engineering, Ann Arbor, MI 48109

Abstract

Discrete multi-load truss sizing optimization (MTSO) problems are challenging to solve due to their combinatorial, nonlinear, and non-convex nature. This study highlights two important characteristics of the feasible set of MTSO problems considered here, in which force balance equations, Hooke's law, yield stress, bound constraints on displacements, and local bucking are taken into account. Namely, we use the linear or bilinear nature of the problem to take advantage of re-scaling properties of both the problem's design and auxiliary variables, as well as to extend the superposition principle to the case in which nonlinear stress constraints are considered. Taking advantage of these characteristics, we extend the neighborhood search mixed-integer linear optimization (NS-MILO) method (Shahabsafa et al., 2018), which provides an effective heuristic solution approach based on exact solution methods for MILO problems. Through extensive computational experiments, we demonstrate that the extended NS-MILO method provides high-quality solutions for large-scale discrete MTSO problems in a reasonable time.

1 Introduction

Truss structures are widely used in a variety of infrastructures like bridges and buildings. A truss design problem is concerned with the optimal design of a truss structure with respect to an objective, e.g., the structure's weight, while considering several mechanical constraints. In a truss design problem, the shape and the topology of the structure, as well as the cross-sectional areas of bars, can be considered (Topping, 1983; Ben-Tal and Bendsøe, 1993). In truss sizing optimization (TSO) problems, the truss topology is given, and the cross-sectional areas of bars are to be decided (Dorn et al., 1964). In real-world applications, a truss structure should withstand different loading conditions. We refer to these problems as *multi-load truss sizing optimization (MTSO)* problems. A variety of models assume that that the cross-sectional areas of the bars can be selected from a continuous range (Stolpe, 2004; Degertekin, 2012); while others consider a more realistic situation in which the cross-sectional areas of the bars are required to belong to a discrete set of options (Achtziger, 1998; Achtziger and Stolpe, 2007a,b,c; Mela, 2014).

Mellaert et al. (2016) proposed a mixed-integer linear optimization (MILO) model for discrete single-load TSO problems considering displacement constraints, member constraints, and joint constraints. Shahabsafa et al. (2018) proposed a MILO model for discrete single-load TSO problems with weight as its objective function. They considered additional physical constraints such as Hooke's law and Euler buckling constraints. In truss topology design (TTD) problems, potential bars can take zero cross-sectional areas. Achtziger (1998) studied the discrete truss topology design and sizing optimization problem with the objective of minimizing the maximum compliance considering multiple load cases. Mela (2014) and Shahabsafa et al. (2021) suggested a MILO model for discrete truss topology design and sizing optimization problems considering physical constraints.

Another class of problems can be reformulated as a MTSO problem; namely, when the structure is under uncertain load cases (Lógó et al., 2009). Stochastic optimization is a mathematical approach to deal with uncertainty by considering random variables in the problem. For example, in special cases, when one has discrete random variables, a stochastic problem can be reformulated as a multi-load problem (Csébfalvi, 2018). Alvarez and Carrasco (2005) demonstrated that the minimum expected compliance under stochastic load cases coincides with the dual of a special convex minimax problem. They proved that the expected compliance minimization problem is equivalent to a multiload problem with a specific finite set of multiple load cases. Makrodimopoulos et al. (2010) proposed a new compliance-based objective for the truss design problem under multiple load cases. Their model minimizes the summation of the maximum strain energy of the structure. They proved that for kinematically stable and determinate structures, the proposed problem is equivalent to a weight minimization problem.

Uncertainty in load cases can also be modeled using robust optimization instead of stochastic optimization (Calafiore and Dabbene, 2008; Zhao and Wang, 2014). In these cases, the problem typically cannot be reformulated as a MTSO problem. Kanno and Takewaki (2006) applied the quadratic embedding method of uncertainty and the S-procedure (Ben-Tal and Nemirovski, 2001) and reformulated the problem as a nonlin-

ear semidefinite optimization problem. Dunning et al. (2011) considered uncertainties in the external loads' magnitude and direction in the compliance minimization problem. They applied an analytical approach for normally distributed external forces and converted the robust optimization problem into a multi-Load problem. Liu and Gea (2018) proposed a new continuous formulation for TTDSO problems where bars are under uncertain loads. The ellipsoid-bounded uncertainty comes from both the external loads' magnitude and direction. The objective is to minimize maximum compliance.

Several authors tried to tackle truss design problems under multiple load cases (see e.g., Lamberti, 2008; Azad and Hasançebi, 2015; Do and Lee, 2017). Smith (1997) extended the heuristic method that is developed by Pedersen (1993) for single-load truss design problems to solve multi-Load topology design and sizing optimization problems. Cheng et al. (2016a) and Lee et al. (2005) proposed a harmony search algorithm to solve discrete MTSO problems. They considered some bounds constraints for yield stress, nodal displacement, and Euler buckling constraints. However, they did not formally show how to relate yield stress and nodal displacement to the bars' cross-sectional areas. Azad and Hasançebi (2014a) developed a neighborhood search meta-heuristic algorithm for discrete MTSO problems without considering Euler buckling constraints. Capriles et al. (2007) and Camp and Farshchin (2014) suggested an ant colony algorithm for the discrete MTSO problems without considering the effect of Euler buckling constraint on the problem. To enforce the physical constraints, they used a penalty function. Stolpe (2016) comprehensively reviewed the methods that were used to solve truss design problems.

This paper presents a methodology that aims to provide high-quality solutions for large-scale MTSO problems. Our proposed methodology is based on exact methodologies. Though it does not warrant globally optimal solutions, it is still a practical heuristic. Throughout the paper, we use the term "high-quality solution" to refer to solutions that are at least equal in quality or better than the best-known solutions to the problem of interest. We consider the minimum-weight MTSO problem with force balance equations, Hooke's law, yield stress bounds, displacement bounds, and Euler buckling constraints (Shahabsafa et al., 2018). We present two crucial characteristics of the feasible set of MTSO problems: (a). Given a feasible truss structure for the continuous MTSO problem, we prove that a proportional scaling of cross-sectional areas, up to their upper bounds, remains feasible for the problem. (b). We also prove that adding any convex combination of existing load cases does not change the feasible set of the MTSO problem. As the size of the truss structures grows, it becomes increasingly difficult to find a proven optimal solution for discrete MTSO problems. To overcome this difficulty, we extend the neighborhood search mixed-integer linear optimization (NS-MILO) method (Shahabsafa et al., 2018), which performs well in providing high-quality solutions for single-load discrete TSO problems, to solve MTSO problems. By solving various classical and large-scale test problems, we demonstrate that the extended NS-MILO method provides high-quality solutions for MTSO problems.

The rest of the article is organized as follows. In Section 2, we formally introduce both the continuous and discrete MTSO problems. In Section 3, we present two essential properties of the feasible set of MTSO problems. In Section 4, we present the exten-

sion of the NS-MILO method for MTSO problems that is an effective heuristic based on MILO methodologies. Then, through extensive computational experiments, we demonstrate the extended NS-MILO method's efficiency in solving large-scale MTSO problems.

2 Problem description

In this article, we consider multi-load TSO problems. Our mathematical optimization model for MTSO problems is a reformulation of the TSO model introduced by Shahabsafa et al. (2018, 2021).

We discuss different dimensions of the problem. Let m and n denote the number of bars and degrees of freedom of the ground structure, respectively. The dimension of the space is denoted by d ($d = 2, 3$). We assume that each node is either fixed in all directions or pinned. Let $\mathcal{I} = \{1, \ldots, m\}$ be the index set of the bars of the ground structure and let $\mathcal{H} = \{1, \ldots, p\}$ represent the index set of the load cases, where p denotes the number of the load cases.

Vector $x \in \mathbb{R}^m_{++}$ denotes the cross-sectional areas of the bars, where $\mathbb{R}^m_{++}$ is the m-dimensional space of strictly positive vectors. Let $f^h \in \mathbb{R}^n$, for $h \in \mathcal{H}$, denote the vector of the external loads in case h. Let $q^h \in \mathbb{R}^m$, for $h \in \mathcal{H}$, represent the vector of the internal loads in case h. The relationship between the external loads and internal loads are governed by the force balance equations (2b), where $R \in \mathbb{R}^{n \times m}$ is the topology matrix of the truss structure.

The stress on bar $i \in \mathcal{I}$ in load case $h \in \mathcal{H}$ is denoted by σ_i^h, and is defined in constraints (2e). Let $u^h \in \mathbb{R}^n$ and $\Delta l^h \in \mathbb{R}^m$, for $h \in \mathcal{H}$, denote the nodal displacements and the elongations of the bars in load case h, respectively. The relationship between the nodal displacements and the elongations of the bars is ensured by constraints (2c): Let E_i and l_i, for $i \in \mathcal{I}$, be the Young's modulus and the length of bar $i \in \mathcal{I}$, respectively. Hooke's law governs the relationship between the stress and elongation of the bars. Constraints (2d) ensure that Hooke's law is satisfied. Let I_i, for $i \in \mathcal{I}$, be the moment of inertia associated with the cross-sectional area of bar i and let y_i, for $i \in \mathcal{I}$, be defined as

$$y_i = \frac{4\pi I_i}{x_i}.$$

The value of y_i can be physically interpreted as the area of a circle with twice the radius of gyration (defined as $\sqrt{I_i/x_i}$) as its radius (see, e.g., Lubliner and Papadopoulos, 2016, Sec. 10.3). Let $\gamma_i = \pi E_i / 4l_i^2$ for $i \in \mathcal{I}$. The Euler buckling constraints can be written as

$$\sigma_i^h \geq -\frac{\pi^2 E_i I_i}{l_i^2 x_i} = -\frac{\pi E_i}{4l_i^2}\frac{4\pi I_i}{x_i} = -\gamma_i y_i, \quad i \in \mathcal{I}, h \in \mathcal{H}. \tag{1}$$

Throughout the article, we consider bars with solid circular cross-sections. In this case, we have that $y_i = x_i$. Thus, the Euler buckling constraints can be written as (2f).

Let $\sigma^{\min}, \sigma^{\max} \in \mathbb{R}^m$ be the lower and upper bounds on the stress of the bars where $\sigma^{\min} < 0 < \sigma^{\max}$. Let $x^{\min}, x^{\max} \in \mathbb{R}^m$ be the lower and upper bounds on the bars'

cross-sectional areas. Also, let $u^{\min}, u^{\max} \in \mathbb{R}^n$ denote the lower and upper bounds of the nodal displacements, respectively. We set $u^{\min} < 0 < u^{\max}$.

Let ρ be the density of the material used to construct the truss structure. The objective is to minimize the structure's total weight, which is equal to $\rho\, l^T x$. The continuous MTSO problem can be formulated as follows:

$$
\begin{aligned}
\min \quad & \rho\, l^T x, && && && \text{(2a)}\\
\text{s.t.} \quad & Rq^h && = f^h, && h \in \mathcal{H}, && \text{(2b)}\\
& R^T u^h && = \Delta l^h, && h \in \mathcal{H}, && \text{(2c)}\\
& \frac{E_i}{l_i}\Delta l_i^h - \sigma_i^h && = 0, && i \in \mathcal{I}, h \in \mathcal{H}, && \text{(2d)}\\
& q_i^h - x_i \sigma_i^h && = 0, && i \in \mathcal{I}, h \in \mathcal{H}, && \text{(2e)}\\
& \sigma_i^h + \gamma_i x_i && \geq 0, && i \in \mathcal{I}, h \in \mathcal{H}, && \text{(2f)}\\
& u^{\min} && \leq u^h \leq u^{\max}, && h \in \mathcal{H}, && \text{(2g)}\\
& \sigma^{\min} && \leq \sigma^h \leq \sigma^{\max}, && h \in \mathcal{H}, && \text{(2h)}\\
& x^{\min} && \leq x \leq x^{\max}. && && \text{(2i)}
\end{aligned}
$$

In model (2), the bars' cross-sectional areas are assumed to be continuous decision variables. However, in practice, due to manufacturing and economic restrictions, bars frequently take values only from a predefined discrete set (Achtziger and Stolpe, 2007a). Without loss of generality, we may assume that the number of candidate sizes is the same for all the bars. Furthermore, we assume that all the bars have the same set $\mathcal{S}$ of potential cross-sectional areas for ease of presentation. Let $\mathcal{S}$ be the set of possible non-zero cross-sectional areas of the bars defined as:

$$\mathcal{S} = \{s_1, s_2, \ldots, s_v\}, \tag{3}$$

where $0 < s_1 \leq s_2 \leq \ldots \leq s_v$ and v is the cardinality of the set $\mathcal{S}$. Let $\mathcal{K} = \{1, \ldots, v\}$ denote the set of indices corresponding to the discrete set $\mathcal{S}$. The cross-sectional area of bar i, for $i \in \mathcal{I}$, takes values from the set $\mathcal{S}$ in the discrete MTSO problem. Next, we apply the *incremental* model proposed by Shahabsafa et al. (2018, 2021) for the discrete single-load TSO problems, to discrete MTSO problem. Let $\bar{\mathcal{K}} = \{1, \ldots, v-1\}$ and $\delta_k = s_{k+1} - s_k$ for $k \in \bar{\mathcal{K}}$. The incremental formulation of choosing from the discrete set of cross-sectional areas is as follows:

$$
\begin{aligned}
& x_i = \sum_{k \in \bar{\mathcal{K}}} \delta_k z_{ik}, && i \in \mathcal{I},\\
& z_{ik} \leq z_{i,k-1}, && i \in \mathcal{I},\ k \in \bar{\mathcal{K}} \setminus \{1\},\\
& z_{ik} \in \{0, 1\}, && i \in \mathcal{I},\ k \in \bar{\mathcal{K}}.
\end{aligned}
\tag{4}
$$

Let σ_{ik}^h, for $i \in \mathcal{I}$, $k \in \mathcal{K}$ and $h \in \mathcal{H}$, be the stress on bar i in load case h if $x_i = s_k$, that is

$$
\sigma_{ik}^h = \begin{cases} \frac{E_i}{l_i}\Delta l_i^h, & \text{if } x_i = s_k;\\ 0, & \text{otherwise.} \end{cases}
$$

Notice that $\sigma_i^h = \sum_{k\in\mathcal{K}} \sigma_{ik}^h$. The following set of constraints enforce yield stress and Euler buckling constraints:

$$\begin{array}{lll} \max\left(-\gamma_i s_1, \sigma_i^{\min}\right)(1-z_{i1}) & \le \sigma_{i1}^h \le \sigma_i^{\max}(1-z_{i1}), & i\in\mathcal{I}, h\in\mathcal{H}, \\ \max\left(-\gamma_i s_k, \sigma_i^{\min}\right)\left(z_{i,k-1}-z_{ik}\right) & \le \sigma_{ik}^h \le \sigma_i^{\max}\left(z_{i,k-1}-z_{ik}\right), & i\in\mathcal{I}, k\in\bar{\mathcal{K}}\setminus\{1\}, h\in\mathcal{H}, \\ \max\left(-\gamma_i s_v, \sigma_i^{\min}\right) z_{i,v-1} & \le \sigma_{iv}^h \le \sigma_i^{\max} z_{i,v-1}, & i\in\mathcal{I}, h\in\mathcal{H}. \end{array} \tag{5}$$

The discrete MTSO problem can then be formulated as:

$$\begin{array}{lllll} \min & \rho\, l^T x, & & & \\ \text{s.t.} & Rq^h & = f^h, & & h\in\mathcal{H}, \\ & R^T u^h & = \Delta l^h, & & h\in\mathcal{H}, \\ & x_i - s_1 - \sum_{k\in\bar{\mathcal{K}}} \delta_k z_{ik} & = 0, & & i\in\mathcal{I}, \\ & \frac{E_i}{l_i}\Delta l_i^h - \sum_{k\in\mathcal{K}} \sigma_{ik}^h & = 0, & & i\in\mathcal{I}, h\in\mathcal{H}, \\ & q_i^h - \sum_{k\in\mathcal{K}} s_k \sigma_{ik}^h & = 0, & & i\in\mathcal{I}, h\in\mathcal{H}, \\ & z_{ik} & \le z_{i,k-1}, & & i\in\mathcal{I},\ k\in\bar{\mathcal{K}}\setminus\{1\}, \\ & u^{\min} & \le u^h & \le u^{\max}, & h\in\mathcal{H}, \\ & \max\left(-\gamma_i s_1, \sigma_i^{\min}\right)(1-z_{i1}) & \le \sigma_{i1}^h & \le \sigma_i^{\max}(1-z_{i1}), & i\in\mathcal{I}, h\in\mathcal{H}, \\ & \max\left(-\gamma_i s_k, \sigma_i^{\min}\right)\left(z_{i,k-1}-z_{ik}\right) & \le \sigma_{ik}^h & \le \sigma_i^{\max}\left(z_{i,k-1}-z_{ik}\right), & i\in\mathcal{I}, k\in\bar{\mathcal{K}}\setminus\{1\}, h\in\mathcal{H}, \\ & \max\left(-\gamma_i s_v, \sigma_i^{\min}\right) z_{i,v-1} & \le \sigma_{iv}^h & \le \sigma_i^{\max} z_{i,v-1}, & i\in\mathcal{I}, h\in\mathcal{H}, \\ & z_{ik}\in\{0,1\}, & & & i\in\mathcal{I},\ k\in\bar{\mathcal{K}}. \end{array} \tag{6}$$

The number of variables and constraints in the continuous MTSO model (2) are $p(3m+n)+m$ and $p(6m+3n)+2m$, respectively. Also, the number of variables and constraints in the discrete MTSO model (6) are $p(2m+n)+mv(p+1)$ and $p(7m+3n)+m(v-2)(2p+1)$, respectively. The number of variables and constraints of model (6) is a third-order polynomial on the size of the problem leading to a large-scale MILO model as the problem size grows. It is worth noting that a formulation of the problem of interest in terms of only the design variables has a much higher level of non-linearity that makes the problem impractical to solve using the discussed optimization approach.

2.1 Circular hollow bars

Our models can be extended to bars with other shapes of cross-sectional areas. Here, we present the adaptation of models (2) and (6) to hollow circular cross-sections. Let us denote by r_i^{in} and r_i^{out}, the inner radius and the outer radius of the circular cross-section of bar $i\in\mathcal{I}$, respectively, and let $x_i^{\text{out}} = \pi {r_i^{\text{out}}}^2$ and $x_i^{\text{in}} = \pi {r_i^{\text{in}}}^2$ denote the outer and inner circular cross-sectional area of bar $i\in\mathcal{I}$. Then, for every bar $i\in\mathcal{I}$, we have

$$y_i = \frac{4\pi I_i}{x_i} = \frac{4\pi\left(\frac{\pi}{4}({r_i^{\text{out}}}^4 - {r_i^{\text{in}}}^4)\right)}{\pi({r_i^{\text{out}}}^2 - {r_i^{\text{in}}}^2)} = \pi({r_i^{\text{out}}}^2 + {r_i^{\text{in}}}^2) = x_i^{\text{out}} + x_i^{\text{in}}. \tag{7}$$

From (1) and (7), the Euler buckling constraints for bars with hollow and circular cross-sections can be written as

$$\sigma_i^h + \gamma_i(x_i^{\text{out}} + x_i^{\text{in}}) \geq 0, \quad i \in \mathcal{I}, h \in \mathcal{H}, \tag{8a}$$
$$x_i - x_i^{\text{out}} + x_i^{\text{in}} = 0, \quad i \in \mathcal{I}, \tag{8b}$$
$$x_i^{\text{in}} \geq 0, \quad i \in \mathcal{I}. \tag{8c}$$

To extend the continuous MTSO model (2) for the bars with hollow cross-sections, it is enough to replace the Euler buckling constraints of the model with constraints (8). Further, to extend the discrete MTSO model (6), we need to replace s_k in the set of constraints (5) with $\bar{s}_k$, for $k \in \mathcal{K}$, where

$$\bar{s}_k = s_k^{\text{out}} + s_k^{\text{in}}.$$

In the rest of the article, we assume that all bars have solid circular cross-sections. In Section 3, we present two important characteristics of the feasible set of the continuous MTSO problem (2), one of which holds for the discrete MTSO problem (6) as well.

3 Theoretical properties of MTSO problems

In this section, we present two essential properties of the feasible set of the MTSO problem (2). These properties are then used in extending the NS-MILO method (Shahabsafa et al., 2018) to provide high-quality solutions for large-scale discrete MTSO problems.

Let $\mathcal{F}$ be the feasible set of the continuous MTSO problem (2) and let $(x, u, \Delta l, \sigma, q) \in \mathcal{F}$ be a feasible solution for problem (2), where

$$\begin{aligned}
u &\coloneqq (u^1, \dots, u^p), & u^h &\in \mathbb{R}^n, & h &\in \mathcal{H}, \\
\Delta l &\coloneqq (\Delta l^1, \dots, \Delta l^p), & \Delta l^h &\in \mathbb{R}^m, & h &\in \mathcal{H}, \\
\sigma &\coloneqq (\sigma^1, \dots, \sigma^p), & \sigma^h &\in \mathbb{R}^m, & h &\in \mathcal{H}, \\
q &\coloneqq (q^1, \dots, q^p), & q^h &\in \mathbb{R}^m, & h &\in \mathcal{H}.
\end{aligned} \tag{9}$$

Let $\mathcal{X}$ denote the m-dimensional subspace of the bars' cross-sectional areas. Additionally, let $\mathcal{F}_\mathcal{X}$ denote the orthogonal projection of the feasible set $\mathcal{F}$ on the subspace $\mathcal{X}$; that is, $\mathcal{F}_\mathcal{X} = \{x \in \mathbb{R}^m_{++} : \exists\, (u, \Delta l, \sigma, q) \text{ s.t. } (x, u, \Delta l, \sigma, q) \in \mathcal{F}\}$. In what follows, the truss structure corresponding to cross-sectional area $x \in \mathbb{R}^m$ is referred to as *structure* x.

3.1 Feasibility along rays

In this section, we demonstrate that any scaling of a feasible structure x for the continuous MTSO problem (2) with coefficient $\alpha \geq 1$ is also feasible for problem (2), if αx satisfies the upper bounds of the cross-sectional areas; that is, $\alpha x \leq x^{\max}$.

Lemma 1 (Kirsch (1993), Sec. 4.2.1) *Let $x \in \mathcal{F}_{\mathcal{X}}$ and $\alpha \geq 1$. If $\alpha x \leq x^{\max}$, then $\alpha x \in \mathcal{F}_{\mathcal{X}}$.*

Lemma 1 does not hold for the discrete MTSO problem (6), since the feasible set of problem (6) is discrete and finite.

To illustrate the feasibility in the rays for the continuous MTSO problem, we consider a simple 5-bar truss structure shown in Figure 1.

Table 1: Parameters of the 5-bar truss structure in Figure 1.

	Bars 1-4	Bar 5
ρ	2.70 g/cm^3	6.52 g/cm^3
E	69 GPa	88 GPa
$\sigma^{\min}$, $\sigma^{\max}$	$\pm$ 172 MPa	$\pm$230 MPa
$u^{\min}$, $u^{\max}$	$\pm$ 1 cm	$\pm$ 1 cm
$x^{\min}$	0.50 cm^2	0.50 cm^2
$x^{\max}$	20 cm^2	20 cm^2

The material properties and the parameters of the 5-bar truss structure are given in Table 1. The structure is subject to two load cases as follows:

1. 3 kN in the negative direction x-axis direction and 3 kN in the positive direction y-axis direction exerted at node 3,

2. 12 kN in the negative direction x-axis direction and 5 kN in the positive direction y-axis direction exerted at node 4.

Bars 1-4 are assumed to have the same cross-sectional areas. The cross-sectional area of bars 1-4 is denoted by x_1 and the cross-sectional area of bar 5 is denoted by x_2.

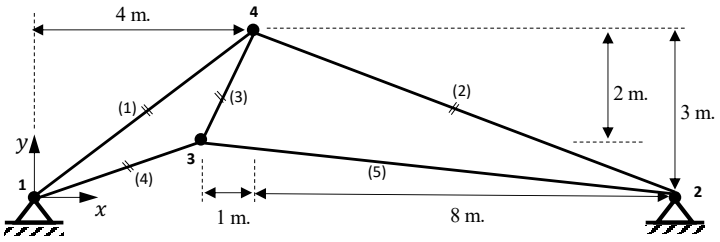

Figure 1: A 5-bar truss structure.

The feasible set projection $\mathcal{F}_{\mathcal{X}}$ of the continuous MTSO problem (2) for the 5-bar truss is plotted in Figure 2. Figure 2, illustrates Lemma 1, that is, if x is feasible for the continuous MTSO problem and $\alpha \geq 1$, then ray αx remains feasible as long as it does not pass the boundary defined by $x_1, x_2 \leq 20$ cm^2.

Figure 2 shows that the feasible set of the continuous MTSO problem for the 5-bar truss is non-convex. Further, it has two local minima $x^\star = (9.75, 0.50)$ cm^2 and $\hat{x} = (5.79, 3.68)$ cm^2. The weights of the structures corresponding to $x^\star$ and $\hat{x}$ are equal to 51.34 and 52.80, respectively. Thus, $x^\star$ is the globally optimal solution of the

problem. We have solved the 5-bar truss problem with the IPOPT solver (Wächter and Biegler, 2006). IPOPT reports $\hat{x}$ as the solution, and thus IPOPT cannot find the globally optimal solution of the problem. The 5-bar truss demonstrates that the feasible set of a truss sizing problem can be non-convex and can have multiple locally optimal solutions.

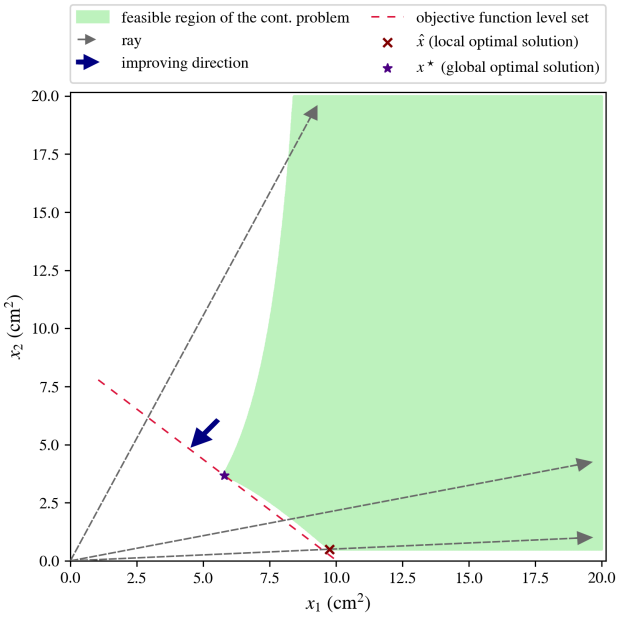

Figure 2: Feasible region of cross-sectional areas of the 5-bar truss structure.

3.2 Convex hull of load cases

Convex combinations of load cases are studied in the shakedown analysis and optimal shakedown design of elasto-plastic trusses under multi-parameter static loading, (see, e.g., Giambanco and Palizzolo, 1995; Kaliszky and Lógó, 2002; Atkočiūnas et al., 2008). The superposition principle states that under linear conditions, a linear combination of sets of feasible stresses corresponding to the load cases satisfies the equilibrium equations for the same combination of the load cases (see, e.g., Lubliner and Papadopoulos, 2016, Sec. 6.2.4). We use the superposition principle to show that a truss structure withstands any load case in the convex hull of load cases extended towards the origin. Adding a convex combination of load cases of the MTSO problem does not change the feasible set of the problem (for a detailed proof, see Fakhimi et al., 2020).

Lemma 2 *Consider MTSO problem (2). Let f^{p+1} be a convex combination of the load cases $\{f^1, f^2, \ldots, f^p\}$, and $\tilde{\mathcal{F}}$ be the feasible set of problem (2) when external load f^{p+1} is added as a new load case; that is, the load cases are given by $\{f^1, \ldots, f^p, f^{p+1}\}$ and $\tilde{\mathcal{H}} := \mathcal{H} \cup \{p+1\}$. Then, $\tilde{\mathcal{F}}_{\mathcal{X}} = \mathcal{F}_{\mathcal{X}}$.*

Corollary 1 is an extension of Lemma 2 where the convex hull of the load cases is extended towards the origin (for a detailed proof, see Fakhimi et al., 2020).

Corollary 1 *Consider the MTSO problem (2) with the set of load cases* $\{f^1, \ldots, f^p\}$. *Let* $\mathcal{F}_{\mathcal{X}}$ *denote the projection of the feasible set on the subspace of the cross-sectional areas. Let* $f^{p+1} = \sum_{h=1}^{p} \lambda_h f^h$, $\sum_{h=1}^{p} \lambda_h \leq 1$, *and* $\lambda_h \geq 0$ *for* $h \in \{1, \ldots, p\}$. *Further, let* $\tilde{\mathcal{F}}_{\mathcal{X}}$ *denote the projection of the feasible set on the subspace of the cross-sectional areas when the load cases are given by* $\{f^1, \ldots, f^p, f^{p+1}\}$. *Then,* $\tilde{\mathcal{F}}_{\mathcal{X}} = \mathcal{F}_{\mathcal{X}}$.

Lemma 2 and Corollary 1 also hold for the discrete MTSO problem (6). Thus, we conclude that adding a load case which is in the convex hull of the existing load cases extended towards the origin does not change the projection of the feasible set to the subspace of the cross-sectional areas of problems (2) and (6), and thus, nor do the optimal cross-sectional areas change. We can use this result to reduce the number of cases in discrete and continuous MTSO problems by eliminating the load cases that are redundant.

3.3 Redundant load case elimination procedure

Consider the following linear feasibility problem:

$$f^{\hat{h}} = \sum_{h \in \mathcal{H} \setminus \hat{h}} \lambda_h f^h, \qquad \sum_{h \in \mathcal{H} \setminus \hat{h}} \lambda_h \leq 1, \qquad \lambda_h \in [0, 1], \quad \forall h \in \mathcal{H} \setminus \hat{h}. \tag{10}$$

The load case $f^{\hat{h}}$, for $\hat{h} \in \mathcal{H}$, can be eliminated, if feasibility problem (10) has a solution. To identify all the load cases that can be eliminated, one can start by solving the feasibility problem (10) for the load case f^1 and eliminate f^1 if the corresponding feasibility problem has a solution, and iteratively do the same for all the remaining load cases.

To illustrate the impact of dependent load cases on the solution time, we solved a series of synthetic discrete MTSO problems for a 2D cantilever instance with 6 blocks[1] with multiple load cases. Specifically, we purposely generate redundant load cases by considering two linearly independent load cases. Then, one-by-one, we add convex combinations of those two load cases to the problem.

We observe that the solution time significantly increases as the number of load cases increases (from 2,277 seconds for two load cases to 199,089 seconds for twelve load cases). Notice though that, as expected from Lemma 2, the optimal objective value of the problem does not change as we add load cases that are convex combinations of the two original load cases. On the other hand, we can apply the redundant load case elimination procedure that is outlined in Section 3.3. By applying the procedure, we eliminate all the dependent load cases in less than 1 second. Thus, the solution time of problem (6) can be reduced up to two orders of magnitude by removing load cases that lay in the convex hull of other load cases.

[1] The 2D cantilever truss structure is detailed in Section 4.2.3.

4 Computational experiments for multi-load TSO problems

In this section, we extend the NS-MILO method developed by Shahabsafa et al. (2018), to provide high-quality solutions for large-scale MTSO problems. Then, we demonstrate through extensive computational experiments that the extended NS-MILO method indeed can provide high-quality solutions for MTSO problems.

4.1 Extension of the NS-MILO method

The NS-MILO method is a neighborhood-search algorithm based on MILO methodologies. The NS-MILO method was proposed by Shahabsafa et al. (2018), to provide high-quality solutions for large-scale truss sizing optimization problems. In the NS-MILO method, we attempt to solve MILO subproblems iteratively. In the MILO subproblems, the size ℓ of the discrete set of each bar is at most $\ell \in \{2, 3, 5\}$.

The NS-MILO method starts by attempting to solve the continuous MTSO problem using a non-linear optimization engine (e.g., IPOPT (Wächter and Biegler, 2006)). Then, it uses the result of Lemma 1 to generate an integer-feasible solution through solving a sequence of MILO_2 subproblems (see Algorithm 1 for details). Having found an initial integer-feasible solution, it attempts to solve a series of MILO_3 subproblems, and ultimately, a series of MILO_5 subproblems. However, none of the MILO_3, nor the MILO_5 subproblems are solved to proven optimality. As soon as a better solution is found, a new MILO subproblem is defined in the neighborhood of the new integer-feasible solution.

The MILO subproblems are denoted by $\text{MILO}_\ell(x)$, where the size of the discrete set of each bar is at most $\ell \in \{2, 3, 5\}$, and $x \in \mathbb{R}^m$ is a vector of cross-sectional areas of the bars. Let $\hat{\mathcal{S}}_i$ be the discrete set of bar i, for $i \in \mathcal{I}$, in subproblem $\text{MILO}_\ell(x)$. The MILO_ℓ ($\ell = 2, 3, 5$) subproblems are defined as follows (Shahabsafa et al., 2018):

1. $\text{MILO}_2(x)$, for $x \in \mathbb{R}^m$, is the discrete MTSO problem (6), where the discrete set of bar i, for $i \in \mathcal{I}$, is defined as

$$\hat{\mathcal{S}}_i := \begin{cases} \{s_k, s_{k+1}\}, & \text{if } \; s_k \leq x_i < s_{k+1}, \\ \{s_{v-1}, s_v\}, & \text{if } \; x_i = s_v. \end{cases}$$

2. $\text{MILO}_3(x)$, for $x_i \in \mathcal{S}$ and $i \in \mathcal{I}$, is the discrete MTSO problem (6), where the discrete set of bar i, for $i \in \mathcal{I}$, is defined as

$$\hat{\mathcal{S}}_i := \begin{cases} \{s_1, s_2\}, & \text{if } \; x_i = s_1, \\ \{s_{k-1}, s_k, s_{k+1}\}, & \text{if } \; x_i = s_k, \; 2 \leq k \leq v-1 \\ \{s_{v-1}, s_v\}, & \text{if } \; x_i = s_v. \end{cases}$$

3. $\text{MILO}_5(x)$, for $x_i \in \mathcal{S}$ and $i \in \mathcal{I}$, is the discrete MTSO problem (6), where the

discrete set of bar i, for $i \in \mathcal{I}$, is defined as

$$\hat{\mathcal{S}}_i \coloneqq \begin{cases} \{s_1, s_2, s_3\}, & \text{if } x_i = s_1, \\ \{s_1, s_2, s_3, s_4\}, & \text{if } x_i = s_2, \\ \{s_{k-2}, s_{k-1}, s_k, s_{k+1}, s_{k+2}\}, & \text{if } x_i = s_k,\ 3 \le k \le v-2, \\ \{s_{v-3}, s_{v-2}, s_{v-1}, s_v\}, & \text{if } x_i = s_{v-1}, \\ \{s_{v-2}, s_{v-1}, s_v\}, & \text{if } x_i = s_v. \end{cases}$$

Although the NS-MILO method proposed by Shahabsafa et al. (2018) provides high-quality solutions for single-load case TSO problems, it may fail in solving multi-load TSO problems.

Finding a tight lower bound for the optimal objective value of this problem is challenging. To extend the NS-MILO method for MTSO problems, we make the following modifications in the NS-MILO method:

(i) Let x_c^* be the solution of the continuous MTSO problem (2) reported by the non-linear solver. In the original NS-MILO method (Shahabsafa et al., 2018), the sequence of $\text{MILO}_2(\alpha x_c^*)$ subproblems may fail in finding an initial feasible solution for the discrete MTSO problem. The reason for the failure is that ray αx_c^*, for $\alpha \ge 1$, may be too close to the boundary of the feasible set that in turn would decrease the likelihood of being able to generate an integer-feasible solution in the neighborhood of ray αx_c^*, for $\alpha \ge 1$, in the MILO_2 subproblems.

To resolve this issue, we modify the NS-MILO method by increasing the lower bound of the cross-sectional areas $x^{\min}$ for the continuous problem (2) to stay away from the boundary of the feasible set of the continuous problem (2) and help MILO_2 subproblems to find an initial integer-feasible solution. This seemingly small change significantly improves the performance of the NS-MILO method.

To illustrate the effect of increasing the lower bound of the cross-sectional areas, we again consider the 5-bar truss problem presented in Figure 1. Suppose the cross-sectional areas of the bars are selected from set $\mathcal{S} = \{0.5, 2, 4, 6, 8.5, 11, 13.5, 16.5, 20\}$ cm^2. Let $\hat{x}$ and $x^\star$ denote the solutions of the continuous MTSO problem for the 5-bar truss problem when $x^{\min} = 0.5$ and $x^{\min} = 2$, respectively. The feasible set of the continuous MTSO problem for the 5-bar truss is depicted in Figure 3. As it can be seen in the figure, ray $\alpha\hat{x}$, for $\alpha \ge 1$, stays close to the boundary of the feasible set, while ray $\alpha x^\star$, for $\alpha \ge 1$, is significantly away from the boundary of the feasible set.

Let $\tilde{P}$ denote the MTSO problem (2), except that $x^{\min}$ is set to the closest value of the discrete set to $s_1 + 0.01(s_v - s_1)$. In the modified NS-MILO method, we start by solving the problem $\tilde{P}$.

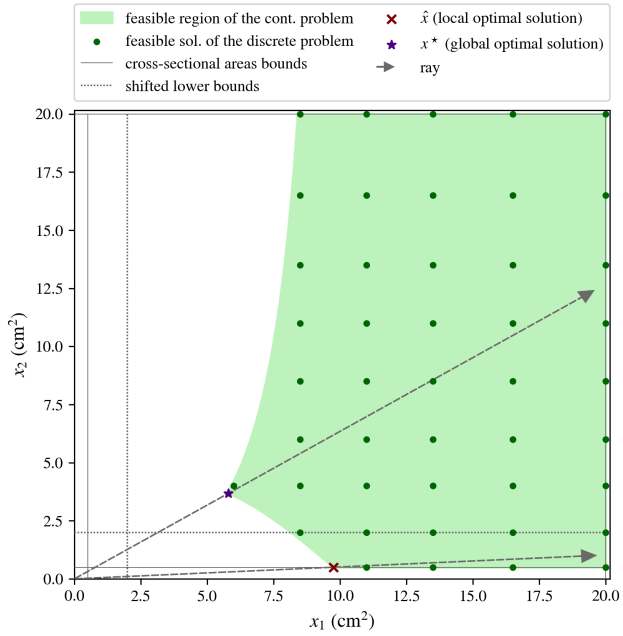

Figure 3: The effect of increasing lower bounds of cross-sectional areas of bars on the search space of the NS-MILO method.

(ii) In the original NS-MILO method (Shahabsafa et al., 2018), a constant time budget is considered in the Gurobi solver for different truss problems. The time budget of the MILO subproblems is set as a function of the size of the subproblems to enable the NS-MILO method to provide high-quality solutions for large-scale multi-load TSO problems. The time budgets of the MILO_2 subproblems are set to pm seconds, where p and m denote the number of load cases and the number of bars, respectively. Additionally, the time budgets of other MILO_ℓ subproblems are set to $dm\ell^2p^2$ seconds, where d is the dimension of the truss.

The outline of the NS-MILO method for MTSO problems is presented in Algorithm 1. The subroutine "Solve$(\cdot)$" returns the best solution of a problem within the time budget. The subroutine "FindSol$(\cdot)$"aims to find an integer-feasible solution with an objective function value better than the initially-fed integer-feasible solution. The solution and the value of the objective function of the MILO subproblems are represented by $\hat{x}$ and $\hat{\eta}$, respectively.

Algorithm 1 The extended NS-MILO method for MTSO problems

$x^0 :=$ solution of problem $\tilde{P}$
$\alpha := 1$
repeat
    $(\hat{x}, \hat{\eta}) :=$ Solve($\text{MILO}_2(\alpha x^0)$)
    $\alpha := \alpha + 0.1$
until a feasible solution is found.
repeat
    $\eta_{\text{curr}} := \hat{\eta}$
    $(\hat{x}, \hat{\eta}) :=$ FindSol($\text{MILO}_3(\hat{x})$)
until $\hat{\eta} = \eta_{\text{curr}}$
repeat
    $\eta_{\text{curr}} := \hat{\eta}$
    $(\hat{x}, \hat{\eta}) :=$ FindSol($\text{MILO}_5(\hat{x})$)
until $\hat{\eta} = \eta_{\text{curr}}$
return $\hat{x}$

4.2 Computational experiments

In this section, we demonstrate how the NS-MILO method solution time scales as the size of an MTSO problem grows. We present computational results for three classical multi-load test problems: the 25-bar space truss of Taye (1987), the 47-bar planar truss of Felix (1981), and the 200-bar planar truss of Thierauf and Cai (1998). Further, we consider scalable large-scale 2D and 3D cantilever and airplane wing truss structures (Shahabsafa et al., 2018). We use the IPOPT solver (Wächter and Biegler, 2006) and Gurobi 9.0.0 (2019) to solve the continuous and discrete optimization models, respectively. We compare the results of the NS-MILO method with the performance of Gurobi when directly applied to model (6). In the following, we use the acronym "Full MILO" when model (6) with the full discrete set (3) is directly solved using Gurobi. As a result, if the Full MILO approach is solved to optimality, then the solution of the Full MILO approach is a global-optimal solution of the problem.

We use a desktop workstation with Dual Intel Xeon® CPU 2630 @ 2.20 GHz (20 cores) and 128 GB of RAM for all the numerical experiments. Both solvers IPOPT and Gurobi are set to use 10 threads. Since Gurobi exhausts memory in solving large-scale discrete MTSO models, the `NodefileStart` parameter is set to 64 GB, which limits the memory usage to that amount. When the memory is at the limit, the nodes are compressed and written to a local disk. Other Gurobi parameters remain at the default values. To make a fair comparison between the Full MILO approach and the NS-MILO method, the time budget of the Full MILO approach is set to be equal to three times the sum of the time budgets of MILO_3 and MILO_5 subproblems, that is, $3(9 + 25)dmp^2 = 102dmp^2$.

4.2.1 The 47-bar planar truss structure

Felix (1981) introduced the 47-bar planar truss structure for the shape and truss sizing optimization problem. Several meta-heuristics algorithms have been applied to the

47-bar truss for the sizing optimization problem (Lee et al., 2011; Kaveh and Mahdavi, 2014; Jalili and Hosseinzadeh, 2018).

Table 2 presents the results for the 47-bar truss structure (for the detailed results, see Fakhimi et al., 2020). Jalili and Hosseinzadeh (2018) found a global optimal solution after 14,400 iterations. However, they did not prove the optimality of the solution, nor did they mention how much time was spent by their algorithm to provide a solution for the problem. The Full MILO approach solves the 47-bar truss structure to proven optimality in 734 seconds. The NS-MILO method can find a globally optimal solution of the problem in 12 seconds (more than 60 times faster).

Table 2: The best published weights (lb) for the multi-load 47-bar planar truss structure.

Design variables	Lee et al. (2011)	Kaveh and Mahdavi (2014)	Jalili and Hosseinzadeh (2018)	Full MILO	NS-MILO
Weight (lb)	2,396.80	2,386.00	2,372.15	2,372.15	2,372.15

4.2.2 The 200-bar planar truss structure

The 200-bar planar truss structure is another well-known large-scale truss structure (Thierauf and Cai, 1998). The results of the 200-bar truss structure are presented in Table 3 (for the detailed results, see Fakhimi et al., 2020). To our best knowledge, the Euler buckling constraints (2f) are not considered for the 200-bar truss structure. Thus, we have compared the NS-MILO method results for the 200-bar truss structure without Euler buckling with the best solutions obtained for the problem in the past. Several meta-heuristics algorithms have been applied to the 200-bar truss for the sizing optimization problem (Azad and Hasançebi, 2014b; Hasançebi and Azad, 2015; Cheng et al., 2016b; Le et al., 2019; Degertekin et al., 2019). The best solution, found so far, for the 200-bar truss problem without Euler buckling constraints has been reported by Cheng et al. (2016b) using the HHS algorithm with the total weight of 27,163 lbs. The NS-MILO method can obtain a lighter solution with a total weight of 26,996 lbs for the same problem in 2,773 seconds. Notice that the Full MILO approach cannot find any solution lighter than 27,527 lbs in 367,200 seconds, which is over 100 times more than the NS-MILO method's solution time.

Further, we have compared the NS-MILO method's performance with that of the Full MILO approach in solving the 200-bar truss problem with the Euler buckling constraints. In the 200-bar truss problem with the Euler buckling constraints, the NS-MILO method stops after 11,151 seconds with a solution of 58,288 lbs. The Full MILO approach finds a heavier structure with a weight of 65,029 lbs in 367,200 seconds that is over 30 times more than the solution time of the NS-MILO method.

Considering the Euler buckling constraints for the 200-bar truss optimization increases the total weight of the structure and the total solution time of the NS-MILO method. The NS-MILO method solves 9 and 10 MILO subproblems to provide high-quality solutions for the 200-bar truss problem with and without considering Euler buckling constraints, respectively. Although the total number of subproblems in both

cases is roughly the same, the solution time of each subproblem is an order of magnitude greater than the case without Euler buckling constraints, which implies that adding the Euler buckling constraints to the 200-bar truss problem makes the problem more difficult for the NS-MILO method. The difference between the weight of the final structures obtained by the NS-MILO and the Full MILO increases when the Euler buckling constraints are added. This observation indicates that adding Euler buckling constraints makes the problem more difficult for the Full MILO approach. One can justify this observation by the fact that the Euler buckling constraints restrict the stress of the bar by its cross-sectional area.

As shown in Table 3, the NS-MILO method outperforms all the existing methods for the 200-bar truss structure problem without and with the Euler buckling constraint in terms of the total weight of the structure. Notice that the Full MILO approach is not able to solve the 200-bar truss problem without and with Euler buckling constraints to optimality in the given time budget.

Table 3: The best published weights (kip) for the multi-load 200-bar planar truss structure.

Groups	w/o Euler buckling							w Euler buckling	
	Azad and Hasanebi (2014b)	Hasanebi and Azad (2015)	Cheng et al. (2016b)	Le et al. (2019)	Degertekin et al. (2019)	Full MILO	NS-MILO	Full MILO	NS-MILO
Weight (kips)	28.075	27.190	27.163	27.421	27.282	27.527	26.996	65.029	58.288

4.2.3 The 2D and 3D cantilever truss structures

The 2D and the 3D cantilever trusses are scalable truss structures (Shahabsafa et al., 2018). In Figure 4, a 2D cantilever with 2 blocks is illustrated. Each block consists of 5 bars and 2 pinned nodes that are linked together. A 3D cantilever truss structures with 2 blocks is also shown in Figure 4 where each block has 20 bars and 4 pinned nodes.

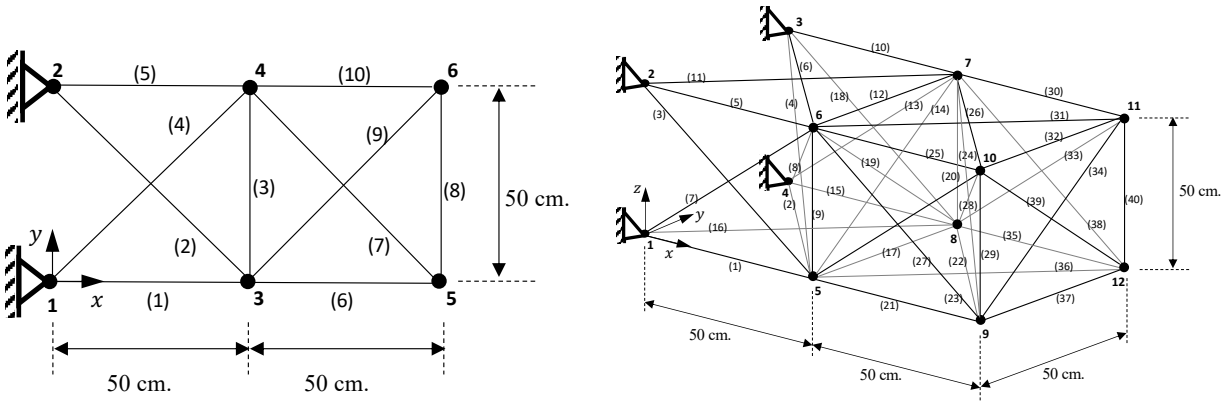

Figure 4: The 2D and 3D cantilever truss structures with two blocks.

In both the 2D and the 3D truss structures, the bar material's density is 2.7 g/cm^3. The Young's modulus of bar material is 69 GPa. The yield stress bounds are $\pm$172.36 MPa.

Let n_b denote the number of blocks. The displacements of nodes must be between $\pm 0.1 n_b^2$ cm except for the 3D cantilever with one block, where the displacement bounds are set to ± 0.25 cm. In both the 2D and the 3D cantilever truss structures, the cross-sectional areas of the bars can be selected from the following set $\mathcal{S} = \{0.25, 0.5, 0.75, 1, 2, 3, 4, 6, 7, 8, 9, 10, 12, 14, 16, 18, 20, 22, 24, 26, 28, 30, 32, 34, 36, 38, 40, 42.5, 45, 47.5, 50, 52.5, 55, 57.5, 60, 62.5, 65, 70, 75, 80, 85\}$ cm^2.

The 2D and 3D cantilever truss structures are subject to two and three load cases, respectively. The load cases for all the 2D and 3D cantilever truss structures are provided in the supplementary material (Fakhimi et al., 2021).

Table 4: Structure weights (kg) and solution times (seconds) for the best solutions found by the Full MILO and the NS-MILO methods for the two-load case 2D cantilever truss structures.

n_b	m	Full MILO			NS-MILO			w_f/w_n
		opt. gap(%)	w_f	t_f	n_2-n_3-n_5	w_n	t_n	
4	20	0.00	10.31	189	1– 6–2	10.31	5	1.00
12	60	11.98	37.18	48,960	1– 9–1	37.15	2,690	1.00
24	120	14.25	88.82	97,920	1–17–1	88.06	22,916	1.01
36	180	16.85	193.83	146,880	1–27–3	190.64	12,472	1.02
48	240	16.82	342.25	195,840	1–28–1	339.20	79,549	1.01
60	300	15.85	474.01	244,800	2–27–1	471.32	73,444	1.01

The results of the Full MILO approach and the NS-MILO method for the two-load case 2D cantilever truss structures are presented in Table 4. It should be noted in that Table 4 "opt. gap" is the ratio of the difference of the best upper and lower bounds of the objective function found by Gurobi divided by the upper bound. In all the cases, the NS-MILO found a solution at least as good as the Full MILO in a smaller amount of time. In Tables 4, 5, and 8, column n_2-n_3-n_5 represents the number of MILO2, MILO3 and MILO5 subproblems, respectively. As the size of the problems grows, the number of subproblems in the NS-MILO method and the optimality gap in the Full MILO approach increases.

Table 5: Structure weights (kg) and solution times (seconds) for the best solutions found by the Full MILO and the NS-MILO methods for the three-load case 3D cantilever truss structures.

n_b	m	Full MILO			NS-MILO			w_f/w_n
		opt. gap(%)	w_f	t_f	n_2-n_3-n_5	w_n	t_n	
1	20	20.88	14.41	55,080	1– 7– 7	14.26	1,337	1.01
3	60	51.11	38.99	165,240	1–12– 1	37.62	75,653	1.04
6	120	67.39	126.85	330,480	2–22– 3	88.02	202,672	1.44
9	180	68.68	252.91	495,720	3–19–10	154.73	541,089	1.63
12	240	70.27	408.67	660,960	3– 9– 8	222.77	311,163	1.83
15	300	82.69	1,019.56	826,200	3– 6–21	315.98	999,078	3.23

The results of the Full MILO approach and the NS-MILO method for the three-load case 3D cantilever truss structures are presented in Table 5. In all the cases, the

NS-MILO method outperforms the Full MILO approach with respect to the solution quality and solution time. In large 3D cantilever problems, the solution quality of the Full MILO drops significantly. The NS-MILO method still provides high-quality solutions in a reasonable amount of time. In the largest instance, the weight of the solution obtained from the Full-MILO method (w_f) is more than three times that of the solution obtained from the NS-MILO method (w_n). Notice in the Full MILO approach that the optimality gap increases rapidly as the problem grows.

We observe that in Tables 4 and 5 the solution time of the NS-MILO method for the 3D cantilever structures is significantly more than that of the NS-MILO method for the 2D cantilever structures with the same number of bars. The 2D cantilever structures are subject to two load cases, while the 3D cantilever structures are subject to three load cases. As mentioned in Section 3.2, the number of load cases significantly impacts the difficulty of discrete MTSO problems. Further, the topologies of the 3D cantilevers are more complicated than that of the 2D cantilevers. These are the reasons that the 3D cantilever problems are significantly more challenging than the 2D cantilever problems. Further, we observe that the ratio w_f/w_n increases from 2D cantilever to 3D cantilever trusses with the same number of bars. This indicates that the Full-MILO approach is adversely affected as the structures get more sophisticated. The NS-MILO method is still able to provide high-quality solutions for those sophisticated structures.

The nodal displacement bound constraints cause the cross-sectional areas of at least one of the bars to decrease in the solutions obtained by the NS-MILO method for all the 2D and 3D cantilever truss structures. In other words, in at least one of the nodes of the solutions obtained by the NS-MILO method, the displacement bounds are active/nearly active. Eliminating the nodal displacement bounds can reduce the solution time of the Full MILO and the NS-MILO methods.

In what follows, a truss structure is denoted by "type–m–p". The "type" can be "2D" and "3D", representing the 2D and the 3D cantilever trusses, respectively. Table 6 illustrates the effect of the nodal displacement bounds on the solution quality for the simplest and the most complicated cantilever truss structures considered in this article, namely, 2D-020-2 and 3D-300-3, respectively. Adding the displacement bound constraints increases the solution time of the Full MILO approach for the 2D-020-2 truss from 71 to 189 seconds. Further, while the weights of the solutions obtained by the NS-MILO method for the 3D-300-3 truss with and without displacement constraints have only about 2% difference (309.84 and 315.98 kg), the weight of the solution of the Full MILO approach for the 3D-300-3 truss with displacement bounds is about 80% more than that of the problem without displacement bounds. This indicates that the Full MILO approach suffers from adding displacement constraints. At the same time, the NS-MILO method finds high-quality solutions for the problem with displacement bound constraints.

Table 6: The impact of the nodal displacement bounds on the solution obtained by the NS-MILO and Full MILO approaches

Problem	Solution methodology	w/o disp. constrs.		w disp. constrs.		
		weight	sol. time	Is active	weight	sol. time
2D-020-2	NS-MILO	9.81	2	Y	10.31	5
	Full MILO	9.81	71	Y	10.31	189
3D-300-3	NS-MILO	309.84	556,910	Y	315.98	999,078
	Full MILO	562.53	826,200	N	1019.56	826,200

4.2.4 Wing truss structures

The airplane wing trusses are 3D truss structures (Shahabsafa et al., 2018). We consider the wing truss structures subject to three load cases: 2.5 g maneuver, -1 g maneuver, and cruise with gust case. The details of these three load cases are given in Table 7. These three cases are based on the data provided by Kenway and Martins (2015); Brooks et al. (2018). The loads are provided as a supplementary material[2].

Table 7: Specifications of three load cases for the wing trusses.

load case	Mach number	Altitude (ft)	Safety factor	Target load MTOW	Actual load MTOW
2.5 g maneuver	0.64	0	1.50	2.5	2.47
-1 g maneuver	0.64	0	1.50	-1.0	-1.01
Cruise with gust	0.86	27,300	2.67	1.3	1.29

The nodal loads over the truss structure are determined using the information provided by Kenway and Martins (2015); Brooks et al. (2018), an aerodynamic solver, and a load transfer solver. Kenway and Martins (2015); Brooks et al. (2018) provide us with the total loads and flight conditions. Then we use AVL, an aerodynamic panel code (Drela and Youngren, 2010), to compute the aerodynamic load over each panel node. We provide AVL with the lift coefficient, C_L, and flight conditions, and AVL will compute the panel nodal load over the panels. For 2.5 g and -1 g maneuver cases, this is simply done by specifying a C_L that could generate 2.5 and -1 times of maximum take-off weight (MTOW). For the cruise case, we follow Brooks et al. (2018) by first setting a C_L to generate unit MTOW, computing the panel loads, and then scaling the loads by 1.3 times. Finally, the loads are transferred to the truss structure from the panels by associating every panel node to the closest truss node. In the process, the forces are directly passed to the structure node. We check the transfer by comparing the actual load with the target load shown in Table 7. We observed about one percent error, which can be ignored in this study.

We consider a conservative approach to activate yield stress and Euler buckling by considering a safety factor for each of the load cases. To do so, we divide the original yield stress and gamma parameter by a suggested safety factor for each of the load cases. The safety factors are also listed in Table 7.

[2]https://github.com/SichengHe/multipoint_crm_avl.git

In all the wing trusses, Young's modulus of the bar material is 69 GPa, and the bar material's density is 2.7 g/cm^3. The yield stress is equal to $\pm$270 MPa. It is assumed that there are no bounds on the nodal displacements of the structure. The load cases and the data of the nodes and bars of the wing structures are provided as supplementary material (Fakhimi et al., 2021). The cross-sectional areas of the bars can be selected from the set $\mathcal{S} = \{0.25, 1, 5, 10, 15, 20, 25, 30, 35, 40, 45, 50, 55, 60, 65, 70, 75, 80, 85, 90, 95, 100, 150, 200, 250, 300, 350, 400, 450, 500, 550, 600, 650, 700, 750, 800, 850, 900, 950, 1000, 1050, 1100, 1150, 1200\}$ cm^2.

In Table 8, the results of the Full MILO approach and the NS-MILO method for the three-load case wing truss structures are provided. As can be seen in the table, the time budget of the Full MILO approach for all the wing trusses is comparable to the solution time of the NS-MILO method. In large cases, the time budget of the Full MILO approach is more than double the solution time of the NS-MILO method. As the size of the wing trusses grows, the optimality gap of the Full MILO approach increases, implying that the Full MILO approach essentially fails in providing high-quality solutions for large-scale wing trusses. However, the relative solution quality of the NS-MILO method and the Full MILO approach (w_f/w_n) increases as the size of the wing truss structures grows. This demonstrates that the NS-MILO method can obtain significantly lighter structures for all the wing trusses. The weight of the 315-bar wing truss obtained by the Full MILO approach is 4.27 times more than that of the solution obtained by the NS-MILO method.

In Table 8, we see that the number of explored branch and bound (B&B) nodes in the NS-MILO method is greater than that of the Full MILO approach. This is because the size of MILO subproblems of the NS-MILO method is smaller than the original MILO problem (6) considered in the Full MILO approach. However, due to the curse of dimensionality, the number of solved subproblems in the NS-MILO method decreases as the size of problems increase.

Table 8: Structure weights (kg) and solution times (seconds) for the best solutions found by the Full MILO and the NS-MILO methods for the three-load case 3D wing truss structures.

m	Full MILO				NS-MILO				w_f/w_n
	Opt. gap(%)	B&B nodes	w_f	t_f	n_2-n_3-n_5	B&B nodes	w_n	t_n	
81	69.02	107,025	90,382.75	223,074	2–29–26	22,523,243	71,991.98	291,231	1.26
117	72.71	33,018	81,609.92	322,218	1–18–17	5,536,400	49,425.86	416,689	1.65
153	64.45	19,678	57,978.18	421,362	2–43– 3	7,738,421	39,367.42	381,712	1.47
207	75.23	13,088	80,244.66	570,078	2–28– 6	1,806,484	32,871.45	619,911	2.44
243	79.82	9,107	97,134.32	669,222	2–18–12	989,296	30,793.12	741,876	3.15
279	82.93	3,694	114,854.71	768,366	2–16– 1	377,198	30,163.22	366,266	3.81
315	84.46	2,162	124,956.18	867,510	2–20– 1	354,607	29,238.46	428,307	4.27

The solution of the 315-bar case is shown in Figure 5. The 2.5 g maneuver case has the most bars with active stress and buckling constraints. However, it only constrains the buckling of the bars for the upper surface. The -1.0 g maneuver case is introduced to constrain the buckling for the bars for the lower surface. The cruise-with-gust case plays a less significant role compared with the 2.5 g maneuver case. The former has

several bars with stress and buckling constraints nearly active because of its higher safety factor.

4.2.5 The modified NS-MILO vs. the original NS-MILO (Shahabsafa et al., 2018)

In this section, we compare the performance of the modified NS-MILO method, proposed in this article, with that of the original NS-MILO method proposed by Shahabsafa et al. (2018). In Table 9, results of the modified NS-MILO method and original NS-MILO method (Shahabsafa et al., 2018) are presented for the largest 2D and 3D cantilever trusses. Here, type "W" stands for wing trusses. As can be seen in the table, the solutions obtained by the original and the modified NS-MILO methods for the 2D cantilever truss with 240 and 300 bars have almost equal objective functions. However, the original NS-MILO method fails in obtaining an integer-feasible solution for the 3D cantilever truss with 300 bars, let alone a high-quality solution, while the modified NS-MILO method can find a high-quality solution. Compared to the original NS-MILO method, the modified NS-MILO method can obtain a solution for the 3D cantilever truss with 240 bars and the 315-bar wing truss that are more than 5 percent lighter. From Table 9, we can see that the modified NS-MILO resolves the issue with finding an initial integer-feasible solution and outperforms the original NS-MILO method in solving large-scale MTSO problems.

Table 9: The structure weights (kg), solution times (seconds) and the number of subproblems for the solutions obtained by the NS-MILO method and the modified NS-MILO method.

problem	NS-MILO (Shahabsafa et al., 2018)			Modified NS-MILO			Improvement
	n_2-n_3-n_5	weight	sol. time	n_2-n_3-n_5	weight	sol. time	in weight %
2D-240-2	1–11– 1	340.09	67,935	1–28– 1	339.20	79,549	0.26
2D-300-2	2– 8– 1	471.41	85,915	2–27– 1	471.32	73,444	0.02
3D-240-3	9–16–27	235.57	1,024,507	3– 9– 8	222.77	311,163	5.75
3D-300-3	—	—	—	3– 6–21	315.98	999,078	∞
W-279-3	5–19– 1	30,267.95	317,731	2–16– 1	30,163.22	366,266	0.35
W-315-3	5–19– 1	30,720.36	476,808	2–20– 1	29,238.46	428,307	5.07

Figure 6 illustrates the solution progress of the modified NS-MILO and the original NS-MILO (Shahabsafa et al., 2018) for the 315-bar wing truss structure. In the NS-MILO method proposed by Shahabsafa et al. (2018), MILO_2 struggles to find an integer-feasible solution. The first integer-feasible solution is in the fifth MILO_2 subproblem in 4,725 seconds, while in the modified NS-MILO method, the first integer-feasible solution is in the second MILO_2 subproblem in 1,890 seconds. The aggregated solution times of MILO_2 and MILO_3 subproblems in the modified NS-MILO method reduce by 60 and 18 percent of those in the original NS-MILO method. In both methods, the MILO_5 subproblem cannot find a better solution, and the algorithm stops. The modified NS-MILO method explores fewer subproblems and is faster in solving the 315-bar wing truss than the original NS-MILO algorithm. The modified NS-MILO

obtains a solution with 29,238.46 kg compared to the solution obtained by the original NS-MILO method with a weight of 30,720.36 kg. Overall, The modified NS-MILO finds a 5 percent lighter structure for the 315-bar wing truss than the original NS-MILO method, with a 10 percent improvement in solution time.

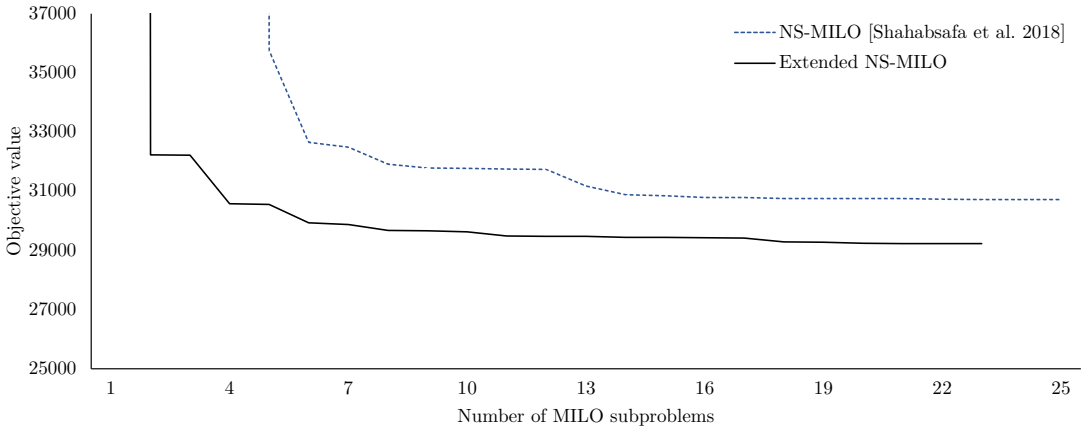

Figure 6: The objective value of the MILO subproblems solved during the NS-MILO method for optimizing wing structure with 315 bars.

4.2.6 The modified NS-MILO vs. the heuristic proposed by Stolpe (2011)

Stolpe (2011) proposed two simple heuristic algorithms to highlight the weakness of so-called intelligent heuristics. The first algorithm consists of two procedures. It initially tries to apply the rounding procedure on a locally optimal solution of the continuous model (2). If the rounded discrete solution is not feasible, it tightens the stress and displacement bounds, and again solves the continuous model.

The algorithm iteratively solves the continuous model, and rounds the obtained solution to the nearest value in the discrete set until an integer-feasible solution is found. Stolpe (2011) did not consider the effect of Euler buckling constraint in his model. To compare this algorithm with the NS-MILO method, we also tighten the Euler buckling constraints in Stolpe's algorithm. To do so, we iteratively decrease value γ in the algorithm until an integer-feasible solution is found. Stolpe (2011) suggested a tightening factor of 0.9995. However, this choice does not stop the algorithm in a reasonable time. Hence, we consider the tightening factor to be equal to 0.99. After finding a feasible solution for the discrete problem, the algorithm tries to reduce the structure's weight by reducing the cross-sectional areas of the bars to the next smallest value for each of the bars. The algorithm selects the bars in decreasing order of potential reduction of the weight of the structure.

We also consider a slightly different variant of the heuristic proposed by Stolpe (2011) that performs better than the original heuristic. In this variant of Stolpe's algorithm, instead of rounding each bar to the nearest discrete value, we round up the continuous problem's solution to find a feasible solution for the discrete MTSO problem (6).

In Table 10, the solutions obtained by a naive rounding procedure, Stolpe's algorithm (Stolpe, 2011), and the improved Stolpe's algorithm are presented. Additionally,

the solution obtained by solving a sequence of MILO_2 subproblems and the final solution of the NS-MILO algorithm are presented. If an algorithm does not lead to a feasible solution for the discrete problem, it is denoted by "–". The column "Norm of diff." is the ℓ_2-norm of the difference of the continuous solution rounded to the nearest integer-feasible solution and the NS-MILO algorithm's final solution.

From Table 10, we can see that the naive rounding procedure fails even for the smallest 2D and 3D cantilever trusses with 20 bars. This indicates the difficulty of finding a feasible solution for the discrete problem from the continuous problem's solution. Stolpe's heuristic (Stolpe, 2011) can find a feasible solution for the smallest 2D and 3D cantilever truss structure instances but fails in providing a feasible solution for large-scale trusses. The improved Stolpe heuristic performs better than the original heuristic but still fails in obtaining a feasible solution for the discrete problem.

As opposed to Stolpe's heuristic, MILO_2 subproblems always lead to a feasible solution for all the test problems considered in this article. Compared to the solutions obtained by Stolpe's heuristic, solving a sequence of MILO_2 subproblems leads to better solutions. The final solutions obtained by the NS-MILO algorithm are significantly better than those obtained by all the other methods.

The last column of the table shows that the final solution obtained by the NS-MILO method is not close to the rounded solution of the continuous problem. This indicates that the NS-MILO method explores the feasible set broadly. Further, in the 315-bar wing truss, the first integer-feasible solution obtained by solving MILO_2 subproblems has a weight of 32,232 kg, and the final solution obtained by the NS-MILO algorithm has a weight of 29,238 kg. Thus, the weight has reduced by 10%, yet another indication that a large neighborhood is explored in the most complex instance considered in the article.

Table 10: Structure weights (kg) and solution times (seconds) for the best solutions found by the heuristic algorithm proposed by Stolpe (2011), its variant, the MILO_2 subproblem and the NS-MILO methods.

Problem	Rounded	Stolpe (2011)		Modified Stolpe (2011)		MILO_2		Modified NS-MILO		Norm
	cont. sol.	Weight	Time	Weight	Time	Weight	Time	Weight	Time	of diff.
2D-020-2	—	18.21	14	11.14	4	10.67	1	10.31	5	4.0
2D-300-2	—	—	138,684	588.20	24,975	504.91	3,007	471.32	73,444	15.0
3D-020-3	—	17.23	16	15.08	3	15.11	1	14.26	1,337	4.0
3D-300-3	—	—	429,406	—	365,990	337.56	16,878	315.98	99,907	24.0
W-081-3	—	—	8,076	—	4,952	74,637.42	27	71,991.98	291231	403.0
W-315-3	—	—	426,458	—	372,552	32,232.35	5,767	29,238.46	428,307	503.0

5 Conclusions and future research

In this paper, we overviewed two important characteristics of multi-load truss sizing optimization (MTSO) problems. We demonstrated that for a given feasible solution of the continuous MTSO problem, an appropriate scaling of cross-sectional areas of the truss structure preserves the feasibility of the new structure for the same problem. This property is used in the neighborhood search mixed-integer linear optimization

(NS-MILO) method. Second, we discussed that adding a convex combination of load cases does not change the feasible set of the MTSO problem. Thus, we can utilize this characteristic to eliminate redundant load cases to reduce the solution time. We also extended the NS-MILO method to provide high-quality solutions for large-scale MTSO problems. Extensive computational experiments confirmed the high performance of the extended NS-MILO method for solving discrete MTSO problems. Further work can be done to extend the formulations to cases where residual stresses, geometric imperfections, and inelastic buckling are considered. Furthermore, extending the results to address other classes of buckling constraints is an interesting direction for future work.

Acknowledgment

This research was supported by Air Force Office of Scientific Research Grant #FA9550-15-1-0222.

References

Achtziger, W. (1998). Multiple-load truss topology and sizing optimization: Some properties of minimax compliance. *Journal of Optimization Theory and Applications*, 98(2):255–280. doi:10.1023/A:1022637216104.

Achtziger, W. and Stolpe, M. (2007a). Global optimization of truss topology with discrete bar areas—part I: theory of relaxed problems. *Computational Optimization and Applications*, 40(2):247–280. doi:10.1007/s10589-007-9138-5.

Achtziger, W. and Stolpe, M. (2007b). Global optimization of truss topology with discrete bar areas—part II: Implementation and numerical results. *Computational Optimization and Applications*, 44(2):315–341. doi:10.1007/s10589-007-9152-7.

Achtziger, W. and Stolpe, M. (2007c). Truss topology optimization with discrete design variables—guaranteed global optimality and benchmark examples. *Structural and Multidisciplinary Optimization*, 34(1):1–20. doi:10.1007/s00158-006-0074-2.

Alvarez, F. and Carrasco, M. (2005). Minimization of the expected compliance as an alternative approach to multiload truss optimization. *Structural and Multidisciplinary Optimization*, 29(6):470–476. doi:10.1007/s00158-004-0488-7.

Atkočiūnas, J., Merkevičiūtė, D., and Venskus, A. (2008). Optimal shakedown design of bar systems: Strength, stiffness and stability constraints. *Computers & Structures*, 86(17):1757–1768. doi:10.1016/j.compstruc.2008.01.008.

Azad, S. K. and Hasançebi, O. (2015). Discrete sizing optimization of steel trusses under multiple displacement constraints and load cases using guided stochastic search technique. *Structural and Multidisciplinary Optimization*, 52(2):383–404. doi:10.1007/s00158-015-1233-0.

Azad, S. K. and Hasançebi, O. (2014a). An elitist self-adaptive step-size search for structural design optimization. *Applied Soft Computing*, 19:226 – 235. doi:10.1016/j.asoc.2014.02.017.

Azad, S. K. and Hasançebi, O. (2014b). An elitist self-adaptive step-size search for structural design optimization. *Applied Soft Computing*, 19:226 – 235. doi:10.1016/j.asoc.2014.02.017.

Ben-Tal, A. and Bendsøe, M. P. (1993). A new method for optimal truss topology design. *SIAM Journal on Optimization*, 3(2):322–358. doi:10.1137/0803015.

Ben-Tal, A. and Nemirovski, A. (2001). *Lectures on Modern Convex Optimization: Analysis, Algorithms, and Engineering Applications*. SIAM. doi:10.1137/1.9780898718829.

Brooks, T. R., Kenway, G. K. W., and Martins, J. R. R. A. (2018). Benchmark aerostructural models for the study of transonic aircraft wings. *AIAA Journal*, 56(7):2840–2855. doi:10.2514/1.j056603.

Calafiore, G. C. and Dabbene, F. (2008). Optimization under uncertainty with applications to design of truss structures. *Structural and Multidisciplinary Optimization*, 35(3):189–200. doi:10.1007/s00158-007-0145-z.

Camp, C. and Farshchin, M. (2014). Design of space trusses using modified teaching–learning based optimization. *Engineering Structures*, 62-63:87 – 97. doi:10.1016/j.engstruct.2014.01.020.

Capriles, P. V. S. Z., Fonseca, L. G., Barbosa, H. J. C., and Lemonge, A. C. C. (2007). Rank-based ant colony algorithms for truss weight minimization with discrete variables. *Communications in Numerical Methods in Engineering*, 23(6):553–575. doi:10.1002/cnm.912.

Cheng, M.-Y., Prayogo, D., Wu, Y.-W., and Lukito, M. M. (2016a). A hybrid harmony search algorithm for discrete sizing optimization of truss structure. *Automation in Construction*, 69:21 – 33. doi:10.1016/j.autcon.2016.05.023.

Cheng, M.-Y., Prayogo, D., Wu, Y.-W., and Lukito, M. M. (2016b). A hybrid harmony search algorithm for discrete sizing optimization of truss structure. *Automation in Construction*, 69:21 – 33. doi:10.1016/j.autcon.2016.05.023.

Csébfalvi, A. (2018). Structural optimization under uncertainty in loading directions: Benchmark results. *Advances in Engineering Software*, 120:68 – 78. doi:10.1016/j.advengsoft.2016.02.006.

Degertekin, S. (2012). Improved harmony search algorithms for sizing optimization of truss structures. *Computers & Structures*, 92-93:229 – 241. doi:10.1016/j.compstruc.2011.10.022.

Degertekin, S., Lamberti, L., and Ugur, I. (2019). Discrete sizing/layout/topology optimization of truss structures with an advanced jaya algorithm. *Applied Soft Computing*, 79:363 – 390. doi:10.1016/j.asoc.2019.03.058.

Do, D. T. and Lee, J. (2017). A modified symbiotic organisms search (msos) algorithm for optimization of pin-jointed structures. *Applied Soft Computing*, 61:683 – 699. doi:10.1016/j.asoc.2017.08.002.

Dorn, W. S., Gomory, R. E., and Greenberg, H. J. (1964). Automatic design of optimal structures. *Journal de Mecanique*, 3:25–52.

Drela, M. and Youngren, H. (2010). *AVL 3.30 User Primer*. MIT. url:http://web.mit.edu/drela/Public/web/avl/avl_doc.txt.

Dunning, P. D., Kim, H. A., and Mullineux, G. (2011). Introducing loading uncertainty in topology optimization. *AIAA Journal*, 49(4):760–768. doi:10.2514/1.J050670.

Fakhimi, R., Shahabsafa, M., and He, S. (2021). Truss-data. url: https://github.com/Fakhimi/truss-data.

Fakhimi, R., Shahabsafa, M., Lei, W., He, S., Martins, J. R. R. A., Terlaky, T., and Zuluaga, L. F. (2020). Large-scale discrete multi-scenario truss sizing optimization: Model analysis and computational methodology experiments. *Lehigh, ISE Department Technical Report*. url: https://engineering.lehigh.edu/sites/engineering.lehigh.edu/files/_DEPARTMENTS/ise/pdf/tech-papers/21/20T_022.pdf.

Felix, J. E. (1981). Shape optimization of trusses subject to strength, displacement, and frequency constraints. Master's thesis, Mechanical Engineering Department, Naval Postgraduate School, USA. url: https://apps.dtic.mil/dtic/tr/fulltext/u2/a114450.pdf.

Giambanco, F. and Palizzolo, L. (1995). Optimality conditions for shakedown design of trusses. *Computational Mechanics*, 16(6):369–378. doi:10.1007/BF00370559.

Gurobi Optimization Inc. (2019). Gurobi optimizer reference manual. url:https://www.gurobi.com.

Hasançebi, O. and Azad, S. K. (2015). Adaptive dimensional search: A new metaheuristic algorithm for discrete truss sizing optimization. *Computers & Structures*, 154:1 – 16. doi:10.1016/j.compstruc.2015.03.014.

Jalili, S. and Hosseinzadeh, Y. (2018). Design optimization of truss structures with continuous and discrete variables by hybrid of biogeography-based optimization and differential evolution methods. *The Structural Design of Tall and Special Buildings*, 27(14):e1495. doi:10.1002/tal.1495.

Kaliszky, S. and Lógó, J. (2002). Plastic behaviour and stability constraints in the shakedown analysis and optimal design of trusses. *Structural and Multidisciplinary Optimization*, 24(2):118–124. doi:10.1007/s00158-002-0222-2.

Kanno, Y. and Takewaki, I. (2006). Sequential semidefinite program for maximum robustness design of structures under load uncertainty. *Journal of Optimization Theory and Applications*, 130(2):265. doi:10.1007/s10957-006-9102-z.

Kaveh, A. and Mahdavi, V. (2014). Colliding bodies optimization method for optimum discrete design of truss structures. *Computers & Structures*, 139:43 – 53. doi:10.1016/j.compstruc.2014.04.006.

Kenway, G. K. and Martins, J. R. R. A. (2015). High-fidelity aerostructural otimization considering buffet onset. In *16th AIAA/ISSMO Multidisciplinary Analysis and Optimization Conference*. American Institute of Aeronautics and Astronautics. doi:10.2514/6.2015-2790.

Kirsch, U. (1993). *Structural Optimization: Fundamentals and Applications*. Springer. doi:10.1007/978-3-642-84845-2.

Lamberti, L. (2008). An efficient simulated annealing algorithm for design optimization of truss structures. *Computers & Structures*, 86(19):1936 – 1953. doi:10.1016/j.compstruc.2008.02.004.

Le, D. T., Bui, D.-K., Ngo, T. D., Nguyen, Q.-H., and Nguyen-Xuan, H. (2019). A novel hybrid method combining electromagnetism-like mechanism and firefly algorithms for constrained design optimization of discrete truss structures. *Computers & Structures*, 212:20 – 42. doi:10.1016/j.compstruc.2018.10.017.

Lee, K., Han, S., and Geem, Z. a. (2011). Discrete size and discrete-continuous configuration optimization methods for truss structures using the harmony search algorithm. *International Journal of Optimization in Civil Engineering*, 1:107–126. url: http://ijoce.iust.ac.ir/article-1-10-en.pdf.

Lee, K. S., Geem, Z. W., ho Lee, S., and woong Bae, K. (2005). The harmony search heuristic algorithm for discrete structural optimization. *Engineering Optimization*, 37(7):663–684. doi:10.1080/03052150500211895.

Liu, J. and Gea, H. C. (2018). Robust topology optimization under multiple independent unknown-but-bounded loads. *Computer Methods in Applied Mechanics and Engineering*, 329:464–479. doi:10.1016/j.cma.2017.09.033.

Lubliner, J. and Papadopoulos, P. (2016). *Introduction to solid mechanics*. Springer. doi:10.1007/978-3-319-18878-2.

Lógó, J., Ghaemi, M., and Rad, M. M. (2009). Optimal topologies in case of probabilistic loading: The influence of load correlation. *Mechanics Based Design of Structures and Machines*, 37(3):327–348. doi:10.1080/15397730902936328.

Makrodimopoulos, A., Bhaskar, A., and Keane, A. J. (2010). A compliance based design problem of structures under multiple load cases. *Structural and Multidisciplinary Optimization*, 42(5):739–743. doi:10.1007/s00158-010-0524-8.

Mela, K. (2014). Resolving issues with member buckling in truss topology optimization using a mixed variable approach. *Structural and Multidisciplinary Optimization*, 50(6):1037–1049. doi:10.1007/s00158-014-1095-x.

Mellaert, R. V., Lombaert, G., and Schevenels, M. (2016). Global size optimization of statically determinate trusses considering displacement, member, and joint constraints. *Journal of Structural Engineering*, 142(2):04015120. doi:10.1061/(ASCE)ST.1943-541X.0001377.

Pedersen, P. (1993). *Topology Optimization of Three-Dimensional Trusses*, pages 19–30. Springer Netherlands, Dordrecht. doi:10.1007/978-94-011-1804-0_2.

Shahabsafa, M., Fakhimi, R., Lei, W., He, S., Martins, J. R. R. A., Terlaky, T., and Zuluaga, L. F. (2021). Truss topology design and sizing optimization with guaranteed kinematic stability. *Structural and Multidisciplinary Optimization*, 63(1):21–38. doi:10.1007/s00158-020-02698-x.

Shahabsafa, M., Mohammad-Nezhad, A., Terlaky, T., Zuluaga, L., He, S., Hwang, J. T., and Martins, J. R. (2018). A novel approach to discrete truss design problems using mixed integer neighborhood search. *Structural and Multidisciplinary Optimization*, 58(6):2411–2429. doi:10.1007/s00158-018-2099-8.

Smith, O. (1997). Topology optimization of trusses with local stability constraints and multiple loading conditions—a heuristic approach. *Structural Optimization*, 13(2):155–166. doi:10.1007/BF01199235.

Stolpe, M. (2004). Global optimization of minimum weight truss topology problems with stress, displacement, and local buckling constraints using branch-and-bound. *International Journal for Numerical Methods in Engineering*, 61(8):1270–1309. doi:10.1002/nme.1112.

Stolpe, M. (2011). To bee or not to bee—comments on "discrete optimum design of truss structures using artificial bee colony algorithm". *Structural and Multidisciplinary Optimization*, 44(5):707–711. doi:10.1007/s00158-011-0639-6.

Stolpe, M. (2016). Truss optimization with discrete design variables: a critical review. *Structural and Multidisciplinary Optimization*, 53(2):349–374. doi:10.1007/s00158-015-1333-x.

Taye, S. (1987). *Approximation concepts in optimum structural design*. PhD thesis, Technion-Israel Institute of technology, Faculty of civil engineering, Israel. url:https://apps.dtic.mil/dtic/tr/fulltext/u2/p000063.pdf.

Thierauf, G. and Cai, J. (1998). Parallelization of the evolution strategy for discrete structural optimization problems. *Computer-Aided Civil and Infrastructure Engineering*, 13(1):23–30. doi:10.1111/0885-9507.00082.

Topping, B. H. V. (1983). Shape optimization of skeletal structures: A review. *Journal of Structural Engineering*, 109(8):1933–1951. doi:10.1061/(ASCE)0733-9445(1983)109:8(1933).

Wächter, A. and Biegler, L. T. (2006). On the implementation of an interior-point filter line-search algorithm for large-scale nonlinear programming. *Mathematical Programming*, 106(1):25–57. doi:10.1007/s10107-004-0559-y.

Zhao, J. and Wang, C. (2014). Robust topology optimization under loading uncertainty based on linear elastic theory and orthogonal diagonalization of symmetric matrices. *Computer Methods in Applied Mechanics and Engineering*, 273:204–218. doi:10.1016/j.cma.2014.01.018.

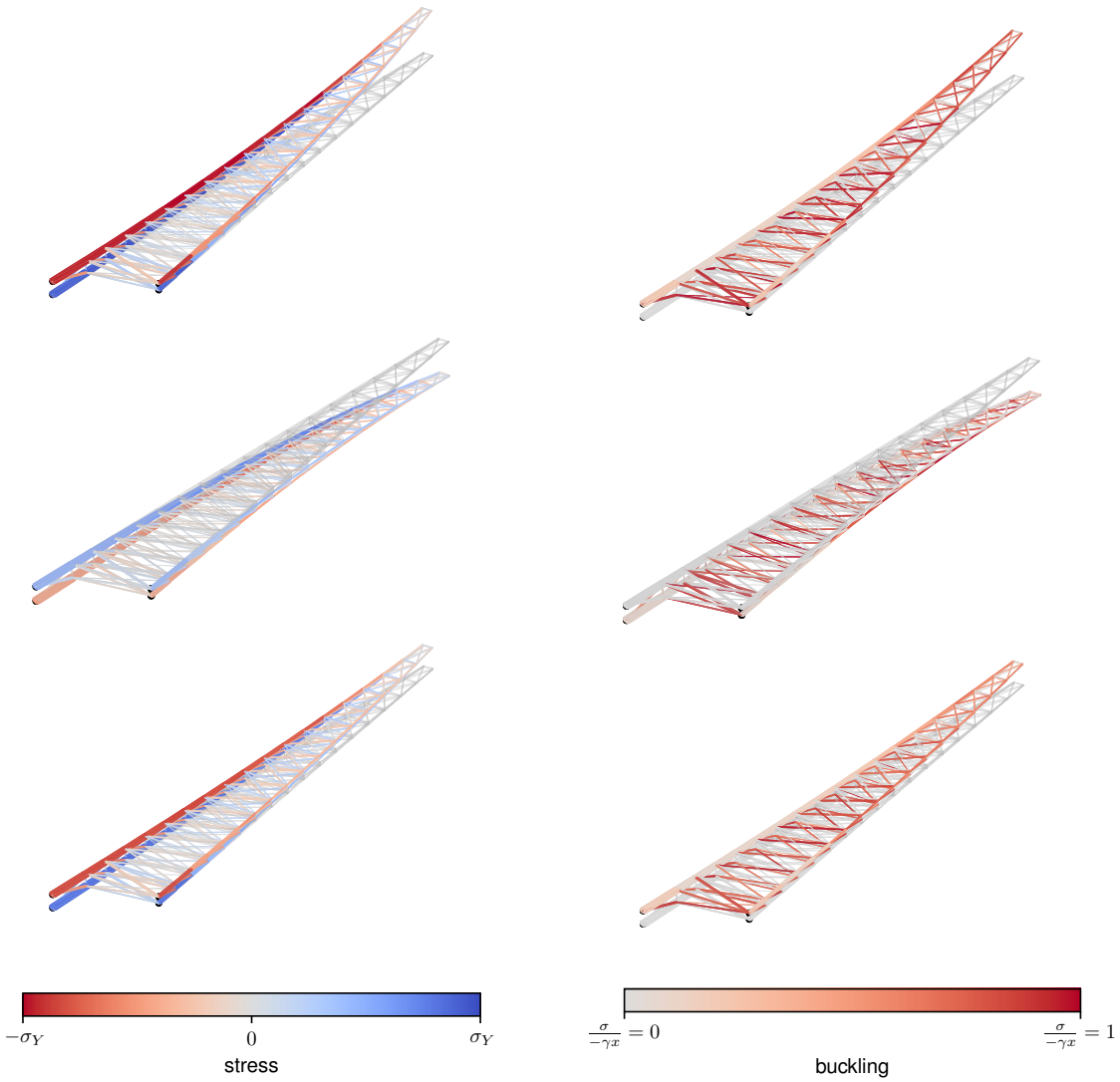

Figure 5: Optimized wing with 315 bars stress and buckling failure parameter distribution under three different load cases, from top to bottom: 2.5 g, -1 g, and cruise load cases. The variables are scaled with safety factors. The undeformed truss is shown in light gray. The buckling failure parameter is set to zero for the bars in tension.